The Astrophysical Journal, 605:921–930, 2004 April 20

THE SOLAR FLARE 3.8–10 keV X-RAY SPECTRUM

K. J. H. Phillips
National Research Council Senior Research Associate, NASA Goddard Space Flight Center, Laboratory for High Energy Astrophysics, Greenbelt, MD 20771; phillips@stars.gsfc.nasa.gov
Received 2003 August 21; accepted 2004 January 6

ABSTRACT

The 3.8–10 keV solar flare spectrum includes lines of highly stripped Ca, Fe, and Ni ions, as well as a continuum steeply falling with energy. Groups of lines at ~7 and ~8 keV, observed during flares by the broadband *RHESSI* spectrometer and called here the Fe line and Fe/Ni line features, are formed mostly of Fe lines but with Ni lines contributing to the ~8 keV feature. Possible temperature indicators of these line features are discussed: the peak or centroid energies of the Fe line feature, the line ratio of the Fe line to the Fe/Ni line features, and the equivalent width of the Fe line feature. The equivalent width is by far the most sensitive to temperature. However, results will be confused if, as is commonly believed, the abundance of Fe varies from flare to flare, even during the course of a single flare. With temperature determined from the thermal continuum, the Fe line feature becomes a diagnostic of the Fe abundance in flare plasmas. These results are of interest for other hot plasmas in coronal ionization equilibrium such as stellar flare plasmas, hot gas in galaxies, and older supernova remnants.

Subject headings: Sun: flares — Sun: X-rays, gamma rays

1. INTRODUCTION

The region 3.8–10 keV ($\lambda = 1.2$–3.3 Å) in solar flare X-ray spectra is of great importance in inferring the properties of the hottest parts of the thermal plasma created during a solar flare. It contains emission lines of highly ionized Ca, Fe, and Ni atoms and a continuum that falls off steeply with increasing energy. Spectra covering this region with broadband energy resolution (FWHM = 0.2–0.8 keV) were obtained by the Soft X-Ray Spectrometer part of the Wide Band Spectrometer on *Yohkoh* (Yoshimori et al. 1991) and the solid-state PIN detector, part of the X-Ray/Gamma-Ray Spectrometer (XGRS) aboard the *Near Earth Asteroid Rendezvous* (*NEAR*) mission (Starr et al. 2000). Most recently, the nine germanium detectors making up *RHESSI* (Lin et al. 2002), launched in 2002 February and continuing to operate at the present time, are observing the solar flare spectrum in the range 3 keV–17 MeV; the spectral resolution in the range 3–10 keV is as high as ~0.8 keV (FWHM) for detector 4. During the flare impulsive stage, a nonthermal continuum is generally evident in *RHESSI* spectra at $E \gtrsim 20$ keV, decreasing much less steeply with E than the thermal continuum and having a power-law dependence (intensity $\propto E^{-\gamma}$). This component is commonly attributed to bremsstrahlung emitted by beamed nonthermal electrons as they travel downward from near the apex of a magnetic loop and lose their energy in the chromosphere or lower corona by Coulomb collisions. Images from *RHESSI* and the Hard X-Ray Telescope (HXT) and Soft X-Ray Telescope (SXT) on *Yohkoh* indicate that the nonthermal bremsstrahlung originates at flare loop footpoints and the thermal plasma is located near or slightly above the loop apex (Lin et al. 2002; Masuda et al. 1994).

The thermal component in *RHESSI* and *NEAR* PIN spectra is observed to have a prominent broadened emission line feature at 7 keV and a less intense line feature at 8 keV indicating high plasma temperatures. The 7 keV feature corresponds to a group of emission lines due to Fe XXV $1s^2$–$1s2l$ ($l = s$, p) lines, associated dielectronic satellites of ions from Fe XIX to Fe XXIV, and fluorescence-formed lines of Fe II, centered on ~6.6 keV, and a second group due to Fe XXVI $1s$–$2p$ (Lyα) lines and associated satellites, centered on ~6.9 keV. The Fe XXV lines are excited at electron temperatures $T_e \gtrsim 12$ MK, while the Fe XXVI lines are excited at $T_e \gtrsim 30$ MK. This line complex is referred to here as the Fe line feature. The 8 keV line feature corresponds to Fe XXV $1s^2$–$1snp$ ($n \geq 3$) lines and Fe XXVI $1s$–np ($n \geq 3$) lines, as well as Ni XXVII $1s^2$–$1s2p$ and Ni XXVIII $1s$–$2p$ lines. We refer to this as the Fe/Ni line feature. Unlike the lines making up the Fe line feature, which have been widely observed, hardly any high-resolution spectra—solar, nonsolar, or laboratory—exist showing the lines making up the Fe/Ni line feature, so *RHESSI* and *NEAR* PIN solar flare observations of the Fe/Ni line feature give unique information about these lines, which have the highest excitation energies in the X-ray spectrum of cosmically abundant elements.

RHESSI observations of the Fe line and Fe/Ni line features, together with those of the thermal continuum, now being routinely made during flares, provide valuable tools in finding T_e and the iron abundance [$A_{\rm flare}({\rm Fe}) = N({\rm Fe})/N({\rm H})$] in flare plasmas. This paper describes the diagnostic capability of these line features, which can be applied to solar flares and nonsolar X-ray sources with similar excitation conditions.

2. LINE EMISSION IN THE 3.8–10 keV RANGE

2.1. *Principal Lines and Their Excitation*

The main ions represented in flare 3.8–10 keV spectra are H-like or He-like Ca, Fe, and Ni ions. (Several Ar and S lines occur between 3.0 and 3.8 keV, which the *RHESSI* energy range extends down to, but we shall not consider them here.) Some early crystal spectrometer observations during large flares (Neupert & Swartz 1970; Neupert 1971; Doschek et al. 1971; Doschek & Meekins 1973) also show weak lines of He-like Ti, Cr, and Mn ions. The thermal component of solar flares has a considerable range of temperatures (see, e.g., Feldman et al. 1995), but generally $T_e < 30$ MK, when the He-like Ca lines (3.86–3.90 keV) and He-like Fe lines and satellites

(6.4–6.7 keV) are the most intense. The resonance lines (w in the notation of Gabriel 1972; sometimes called He α) of Ca XIX, Fe XXV, and Ni XXVII are due to $1s^2\ ^1S_0$–$1s2p\ ^1P_1$ transitions. Intercombination and forbidden lines also occur, on the low-energy side of each w line; their transitions are (in decreasing energy) $1s^2\ ^1S_0$–$1s2p\ ^3P_{1,2}$ (lines y, x) and $1s^2\ ^1S_0$–$1s2s\ ^3S_1$ (line z). Higher excitation lines with transitions $1s^2\ ^1S_0$–$1snp\ ^1P_1$ ($n \geq 3$) occur at progressively higher energies and decreasing intensities. Lyman series lines emitted by H-like Ca, Fe, and Ni also occur in this range. The Fe XXVI Lyα lines, for example, are weak at $T_e < 30$ MK but are comparable in intensity to Fe XXV line w at $T_e \gtrsim 80$ MK.

Satellite lines occur on the low-energy side of the H-like and He-like ion resonance lines. Those near the He-like ion w lines are due to $1s^2nl$–$1s2pnl$ ($n \geq 2, l = s, p$, etc.) in Li-like ions and equivalent transitions in lower ionization stages. The doubly excited $1s2pnl$ states are formed by dielectronic recombination or (for some $n = 2$ satellites) inner shell excitation. Li-like ion satellites with transitions $1s^2nl$–$1s2pnl$ ($n \geq 4$) are decreasingly separated from line w for increasing n. The most intense $n = 2$ Li-like ion satellites are labeled a, j, k ($1s^22p\ ^2P$–$1s2p^2\ ^2D$ transitions), q, r, s, and t ($1s^22s\ ^2S$–$1s2s2p\ ^2P$,^4P transitions), and $d13$/$d15$ ($1s^23p\ ^2P$–$1s2p3p\ ^2D$ transitions). Other Li-like ion satellites due to $1s^2nl$–$1snl3p$, $1s^2nl$–$1snl4p$, etc., transitions occur on the low-energy side of the He-like Ca and Fe ion lines $1s^2$–$1s3p$, $1s^2$–$1s4p$ (Heβ, Heγ), etc., the most intense being those with transitions $1s^22p\ ^2P_{3/2}$–$1s2p(^3P)3p\ ^2D_{5/2}$ (Boiko et al. 1978; Kato et al. 1997). Satellites j, k, and q are comparable in intensity to line w for Fe and Ni at $T_e \lesssim 15$ MK. Satellites emitted by Be-like to C-like ions (transitions $1s^22s^22p^n$–$1s2s^22p^{n+1}$) occur in groups for each ionization stage. For Fe XXIII–Fe XIX lines, these groups are $\sim$0.03 keV wide and occur at approximately 6.62, 6.59, 6.55, 6.51, and 6.48 keV (Doschek et al. 1981; Phillips et al. 1983). Lower ionization stages are represented by pairs of lines that for ions with only a few missing electrons are unresolvable from the Fe II Kα doublet (Palmeri et al. 2003; see below). Similarly, He-like ion satellite lines with transitions $1s2l$–$2l2l'$ ($l, l' = s, p$), all formed by dielectronic recombination, occur on the low-energy side of the Lyα doublet. Several satellites (the most intense being $1s2p\ ^1P_1$–$2p^2\ ^1D_2$ and $1s2p\ ^3P_1$–$2p^2\ ^3P_0$) coincide to form a single intense line feature known as J (Doschek, Kreplin, & Feldman 1979; Dubau et al. 1981).

A few lines are formed by fluorescence of the photosphere by the soft X-ray thermal plasma in the corona. They are emitted when one of the two $1s$ electrons in neutral or once-ionized Fe and Ni atoms in the photosphere is removed by photons with energies greater than the K-shell binding energy I_K (7.11 keV for Fe, 8.33 keV for Ni), followed by a radiative transition from the $2p$ shell (Kα doublet, lines at 6.400, 6.387 keV) or $3p$ shell (Kβ lines). De-excitation may also proceed by rearrangement of the atom and emission of an Auger electron. The fluorescence yield (relative probability of the radiative transition) ω_K increases approximately as Z^4 (Z is atomic number) and so is much greater for Fe and Ni than for lighter elements. Free electrons with energies greater than I_K, such as are abundant in the nonthermal electron population present at the flare impulsive stage, may also K-shell ionize these atoms (Phillips & Neupert 1973), but observations show that fluorescence dominates (Bai 1979; Parmar et al. 1984; Emslie, Phillips, & Dennis 1986; Phillips et al. 1994).

High-resolution ($E/\Delta E \gtrsim 4000$) solar flare spectra covering the H-like and He-like Ca and Fe $n = 1$–2 lines and lower ionization stages have been obtained with Bragg crystal spectrometers aboard *P78-1* (Doschek et al. 1980), *Solar Maximum Mission* (*SMM*; Acton et al. 1980), *Hinotori* (Tanaka 1986), *Yohkoh* (Culhane et al. 1991), and *Coronas-F* (Sylwester et al. 2002). High-resolution He-like Fe and Ni spectra from tokamak plasmas were obtained with crystal spectrometers by Bitter et al. (1979, 1991) and Bombarda et al. (1988). Generally these spectrometers had small energy ranges that included only the lines of interest, e.g., the *Yohkoh* spectrometer observed the regions near the Ca XIX and Fe XXV w lines and the Fe XXVI Lyα doublet.

In Table 1 we give details of the principal lines in the range 3.859–10.349 keV. Their approximate relative importance is indicated by calculated intensities from the Chianti code (Dere et al. 1997; Young et al. 2003) at two temperatures, 20 MK (typical of a solar flare) and 100 MK (observed in some nonsolar sources). The version of Chianti used here (ver. 4.2) corrects earlier errors in software and wavelengths of Fe satellite lines and the free-free continuum.

2.2. *Lines Making up the* Fe *Line and* Fe/Ni *Line Features*

We now discuss the individual lines making up the Fe line and Fe/Ni line features and their contribution functions, i.e., the dependence on T_e of their emission per unit volume emission measure $\int_V N_e^2\, dV$ (N_e is electron density, V is source volume). The Fe line feature is here defined as the excess above the continuum, as observed by a spectrometer with resolution FWHM ≈ 0.8 keV, in the range 5.8–7.5 keV, and the Fe/Ni line feature in the range 7.5–9.2 keV. We calculate the contribution functions in the form of fluxes (photons cm^{-2} s^{-1}) at the distance of Earth (1 AU $= 1.5 \times 10^{13}$ cm) for an emission measure of 10^{49} cm^{-3}. Figure 1 includes the contribution functions of some of the more significant of the lines considered; the details are described below. Note that we take ion temperatures $T_{\rm ion}$ to be equal to T_e on the basis that equilibration times for a wide range of conditions ($T_e = 10$–50 MK, $N_e \gtrsim 3 \times 10^{10}$ cm^{-3}) are less than 10 s (Spitzer 1962), i.e., less than the timescale of the thermal component of most flares.

Fe XXV line w (6.699 keV) is the most intense single line in the energy range of the Fe line feature for a wide range of T_e. The line emission is almost entirely due to direct collisional excitation from the ground state, with a small proportion (ϵ) due to cascades, unresolved dielectronic satellites, and excitation by recombination from H-like Fe. The intensity is given by

$$I_w = (1+\epsilon)\frac{N(\mathrm{Fe}^{+24})N_e V}{4\pi(1\ \mathrm{AU})^2} \times \frac{8.63\times10^{-6}\Upsilon\exp(-E_0/k_{\rm B}T_e)}{T_e^{1/2}}\ \mathrm{photons\ cm^{-2}\ s^{-1}}, \quad (1)$$

where $N(\mathrm{Fe}^{+24})$ is the number density of He-like Fe ions, $k_{\rm B}$ is Boltzmann's constant, and E_0 and Υ are, respectively, the excitation energy and the temperature-averaged collision strength of the transition.

The atomic data discussed by Phillips et al. (2004), based on Bely-Dubau et al. (1982) and ***R***-matrix collisional excitation rates (Kimura et al. 2000), were used to calculate I_w. Expressing $N(\mathrm{Fe}^{+24}) = N(\mathrm{Fe}^{+24})/N(\mathrm{Fe})A_{\rm flare}(\mathrm{Fe})N(\mathrm{H})$, we took the ion fractions of Mazzotta et al. (1998) and a coronal Fe abundance relative to H, $A_{\rm cor} = 1.26 \times 10^{-4}$ (Feldman & Laming 2000) for $A_{\rm flare}$. Lines x, y, and z (6.63–6.68 keV) are partly formed by collisional excitation from the He-like ion's

TABLE 1

SOLAR FLARE LINES IN THE 3.8–10 keV RANGE

ION	ENERGY[b] (keV)	WAVELENGTH[b] (Å)	TRANSITION[c]	LINE LABEL[d]	INTENSITY[a] 20 MK	INTENSITY[a] 100 MK
Ca XIX	3.859	3.2131	$1s^2\ ^1S_0-1s2s\ ^3S_1$	z	80	2
Ca XVIII	3.860	3.2118	$1s^22p\ ^2P_{3/2}-1s2p^2\ ^2D_{5/2}$	j	...	...
	3.865	3.2081	$1s^22p\ ^2P_{1/2}-1s2p^2\ ^2D_{3/2}$	k	...	...
	3.869	3.2045	$1s^22s\ ^2S_{1/2}-1s2p2s(^1P)\ ^2P_{1/2}$	r	...	...
	3.872	3.2023	$1s^22s\ ^2S_{1/2}-1s2p2s(^1P)\ ^2P_{3/2}$	q	...	...
Ar XVII	3.875	3.1996	$1s^2\ ^1S_0-1s4p\ ^1P_1$	Heγ	...	...
Ca XIX	3.881	3.1945	$1s^2\ ^1S_0-1s2p\ ^3P_1$	y	40	1
	3.885	3.1910	$1s^2\ ^1S_0-1s2p\ ^3P_2$	x	40	1
Ca XVIII	3.897	3.1812	$1s^23p\ ^2P_{3/2}-1s2p(^1P)3p\ ^2D_{5/2}$	$d13$	...	...
	3.899	3.1801	$1s^23p\ ^2P_{1/2}-1s2p(^1P)3p\ ^2D_{3/2}$	$d15$	...	...
Ca XIX	3.901	3.1781	$1s^2\ ^1S_0-1s2p\ ^1P_1$	w	250	5
Ar XVIII	3.935	3.1506	$1s\ ^2S_{1/2}-3p\ ^2P_{3/2,1/2}$	Lyβ	7	1
Ar XVII	3.964	3.128	$1s^2\ ^1S_0-1s5p\ ^1P_1$	Heδ	...	...
Ca XIX	4.068	3.048	$1s2p\ ^1P_1-2p^2\ ^1D_2$	J	...	...
Ca XX	4.100	3.0239	$1s\ ^2S_{1/2}-2p\ ^2P_{1/2}$	Lyα_2	5	5
	4.108	3.0185	$1s\ ^2S_{1/2}-2p\ ^2P_{3/2}$	Lyα_1	10	10
K XVIII	4.122	3.008	$1s^2\ ^1S_0-1s3p\ ^1P_1$	Heβ	...	...
Ar XVIII	4.150	2.9875	$1s\ ^2S_{1/2}-4p\ ^2P_{3/2,1/2}$	Lyγ	...	...
K XIX	4.387	2.826	$1s\ ^2S_{1/2}-3p\ ^2P_{3/2,1/2}$	Lyβ	...	...
Ca XVIII	4.509	2.750	$1s^22p\ ^2P_{3/2}-1s2p3p\ ^2D_{5/2}$	Sat.	...	...
Ca XIX	4.578	2.708	$1s^2\ ^1S_0-1s3p\ ^3P_1$	...	...	...
	4.582	2.706	$1s^2\ ^1S_0-1s3p\ ^1P_1$	Heβ	15	...
	4.819	2.573	$1s^2\ ^1S_0-1s4p\ ^1P_1$	Heγ	...	...
Ca XX	4.863	2.5494	$1s\ ^2S_{1/2}-3p\ ^2P_{3/2,1/2}$	Lyβ	5	2
Ca XIX	4.932	2.514	$1s^2\ ^1S_0-1s5p\ ^1P_1$	Heδ	...	...
Ca XX	5.129	2.4174	$1s\ ^2S_{1/2}-4p\ ^2P_{1/2,3/2}$	Lyγ	...	...
	5.252	2.3609	$1s\ ^2S_{1/2}-5p\ ^2P_{1/2,3/2}$	Lyδ	...	...
Fe II	6.391	1.9400	$[1s\ ^2S_{1/2}]-[2p\ ^2P_{1/2}]$	Kα_2	...	...
	6.404	1.9360	$[1s\ ^2S_{1/2}]-[2p\ ^2P_{3/2}]$	Kα_1	...	...
Fe XIX	6.478	1.914	$1s^22s^22p^4\ ^3P_2-1s2s^22p^5\ ^3P_2$	Sat.	...	...
Fe XX	6.505	1.906	$1s^22s^22p^3\ ^4S_{3/2}-1s2s^22p^4\ ^4P_{5/2}$	Sats.	...	...
	6.515	1.903	$1s^22s^22p^3\ ^2D_{3/2}-1s2s^22p^4\ ^2D_{3/2}$	Sats.	...	...
Fe XXI	6.543	1.895	$1s^22s^22p^2\ ^3P_1-1s2s^22p^3\ ^3D_2$	Sats.	...	...
	6.550	1.893	$1s^22s^22p^2\ ^3P_0-1s2s^22p^3\ ^3D_1$	Sats.	...	...
Fe XXII	6.584	1.883	$1s^22s^22p\ ^2P_{3/2}-1s2s^22p^2\ ^2D_{5/2}$	Sats.	...	...
	6.591	1.881	$1s^22s^22p\ ^2P_{1/2}-1s2s^22p^2\ ^2D_{3/2}$	Sats.	...	...
Fe XXIII	6.598	1.879	$1s^22s2p\ ^1P_1-1s2s2p^2(^1D)\ ^1D_2$	r	...	...
	6.609	1.876	$1s^22s2p\ ^3P_2-1s2s2p^2(^1D)\ ^3D_3$	n	...	...
	6.616	1.874	$1s^22s2p\ ^3P_1-1s2s2p^2(^1D)\ ^3D_2$	k	...	...
	6.620	1.873	$1s^22s2p\ ^3P_1-1s2s2p^2(^1D)\ ^3D_1$	i	...	...
	6.627	1.871	$1s^22s^2\ ^1S_0-1s2s^22p(^2S)\ ^1P_1$	β	10	...
Fe XXV	6.634	1.8689	$1s^2\ ^1S_0-1s2s\ ^3S_1$	z	40	40
Fe XXIV	6.642	1.8666	$1s^22p\ ^2P_{1/2}-1s2p^2\ ^2D_{5/2}$	j	...	...
	6.652	1.8638	$1s^22p\ ^2P_{1/2}-1s2p^2\ ^2D_{3/2}$	k	...	...
	6.660	1.8617	$1s^22s\ ^2S_{1/2}-1s2p(^1P)2s\ ^2P_{3/2}$	q	...	...
Fe XXV	6.665	1.8602	$1s^2\ ^1S_0-1s2p\ ^3P_1$	y	30	30
Fe XXIV	6.675	1.8575	$1s^22s\ ^2S_{1/2}-1s2s2p\ ^2P_{1/2}$	t	...	...
Fe XXV	6.680	1.8561	$1s^2\ ^1S_0-1s2p\ ^3P_2$	x	20	20
	6.694	1.8522	$1s^23p\ ^2P-1s2p(^1P)3p\ ^2D$	$d13$, $d15$	...	...
	6.699	1.8508	$1s^2\ ^1S_0-1s2p\ ^1P_1$	w	100	100
	6.920	1.7917	$1s2p\ ^1P_1-2p^2\ ^1D_2$	J^f	...	5
	6.942	1.7861	$1s2s\ ^1S_0-2s2p\ ^1P_1$	Sat.	...	...
Fe XXVI	6.952	1.7834	$1s\ ^2S_{1/2}-2p\ ^2P_{1/2}$	Lyα_2	...	20
	6.973	1.7780	$1s\ ^2S_{1/2}-2p\ ^2P_{3/2}$	Lyα_1	...	40
Fe II	7.058	1.7566	$[1s]-[3p]^b$	Kβ	...	...
Ni XXVII	7.729	1.6042	$1s^2\ ^1S_0-1s2s\ ^3S_1$	z	...	1
	7.764	1.5970	$1s^2\ ^1S_0-1s2p\ ^3P_1$	y	...	1
Fe XXIV	7.783	1.593	$1s^22p\ ^2P_{3/2}-1s2p3p\ ^2D_{5/2}$	Sat.	...	...
Ni XXVII	7.784	1.5929	$1s^2\ ^1S_0-1s2p\ ^3P_2$	x	...	...
	7.804	1.5887	$1s^2\ ^1S_0-1s2p\ ^1P_1$	w	2	5
Fe XXV	7.874	1.5747	$1s^2\ ^1S_0-1s3p\ ^3P_1$	...	...	...
	7.881	1.5732	$1s^2\ ^1S_0-1s3p\ ^1P_1$	Heβ	5	10
Ni XXVII	8.046	1.541	$1s2p\ ^1P_1-2p^2\ ^1D_2$	J	...	...

TABLE 1—*Continued*

Ion	Energy[b] (keV)	Wavelength[b] (Å)	Transition[c]	Line Label[d]	Intensity[a] 20 MK	Intensity[a] 100 MK
Ni XXVIII.....	8.073	1.5358	$1s\ ^2S_{1/2}-2p\ ^2P_{1/2}$	Lyα_2	...	1
	8.102	1.5303	$1s\ ^2S_{1/2}-2p\ ^2P_{3/2}$	Lyα_1	...	2
Fe XXVI	8.246	1.5024	$1s\ ^2S_{1/2}-3p\ ^2P_{1/2}$	Lyβ_2	...	3
	8.252	1.5035	$1s\ ^2S_{1/2}-3p\ ^2P_{3/2}$	Lyβ_1	...	6
Fe XXV	8.296	1.4945	$1s^2\ ^1S_0-1s4p\ ^1P_1$	Heγ	...	3
	8.486	1.461	$1s^2\ ^1S_0-1s5p\ ^1P_1$	Heδ	...	1
	8.592	1.443	$1s^2\ ^1S_0-1s6p\ ^1P_1$	Heϵ	...	...
Fe XXVI	8.700	1.4251	$1s\ ^2S_{1/2}-4p\ ^2P_{3/2,1/2}$	Lyγ	...	3
	8.907	1.392	$1s\ ^2S_{1/2}-5p\ ^2P_{3/2,1/2}$	Lyδ	...	1
Ni XXVII	9.175	1.3514	$1s^2\ ^1S_0-1s3p\ ^3P_1$	...	...	...
	9.183	1.3501	$1s^2\ ^1S_0-1s3p\ ^1P_1$	Heβ	...	...
	9.664	1.283	$1s^2\ ^1S_0-1s4p\ ^1P_1$	Heγ	...	...
	9.887	1.254	$1s^2\ ^1S_0-1s5p\ ^1P_1$	Heδ	...	...
	10.015	1.238	$1s^2\ ^1S_0-1s6p\ ^1P_1$	Heϵ	...	...
Ni XXVIII.....	10.105	1.227	$1s\ ^2S_{1/2}-4p\ ^2P_{3/2,1/2}$	Lyγ	...	...
	10.349	1.198	$1s\ ^2S_{1/2}-5p\ ^2P_{3/2,1/2}$	Lyδ	...	...

[a] Intensities are approximate relative peak intensities (Fe XXV *w* line = 100), as observed by a spectrometer with energy resolution ~0.01 keV, and are from Chianti (ver. 4.2) calculated spectra.

[b] Line energies (wavelengths) from Hata & Grant 1982, 1984; Sevier 1979; Ermolaev & Jones 1973; Erickson 1977; Doschek et al. 1979.

[c] For inner shell (fluorescence) lines, square brackets indicate hole transitions.

[d] Line labels: Gabriel 1972 for He-like Ca, Fe, and Ni; Heβ stands for $1s^2-1s3p$, etc.; Hata & Grant 1984 for Fe XXIII satellites; Ly = Lyman series; other dielectronic satellites indicated by "Sat." or "Sats." (when several satellites occur, the mean energy is given).

ground state but with contributions from recombination of the H-like ion (at higher T_e) and (for line *z*) inner shell ionization of the Li-like ion. Their intensities are smaller than that of line *w*.

Satellite lines formed by dielectronic recombination (e.g., *j*) have intensities (Bely-Dubau et al. 1982)

$$I_s = \frac{N(\mathrm{Fe}^{+24})N_e V}{4\pi(1\ \mathrm{AU})^2}\frac{2.07\times10^{-16}F_s}{T_e^{3/2}}\exp\left(\frac{-E_s}{k_\mathrm{B}T_e}\right)\ \mathrm{photons\ cm^{-2}\ s^{-1}}, \quad (2)$$

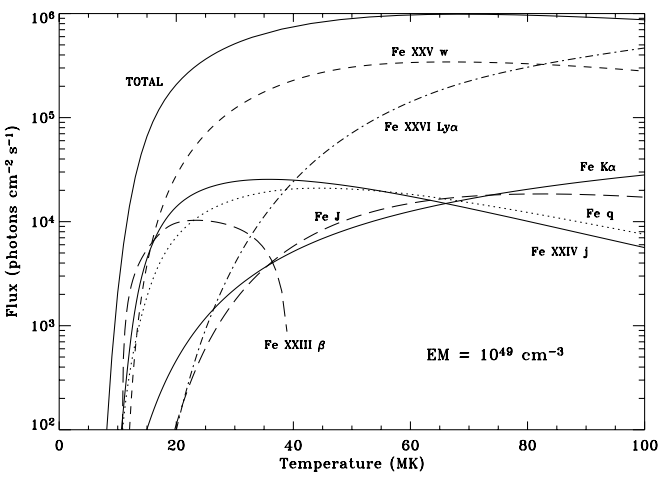

FIG. 1.—Contribution of principal emission lines (labeled) making up the 7 keV Fe line feature. The curve labeled "Total" is the total emission in the line feature between 5.8 and 7.5 keV as estimated from Chianti (ver. 4.2). A coronal (Feldman & Laming 2000) abundance of Fe was assumed for all lines except Fe Kα lines, for which a photospheric Fe abundance (Grevesse & Sauval 1998) was assumed. Curves marked "Fe q" and "Fe J" are those of the Fe XXIV *j* satellite and the Fe XXV satellite feature *J*. The curve marked "Fe Kα" is that due to the Kα fluorescence lines of Fe II. Fluxes are given for an emission measure of 10^{49} cm^{-3}.

where

$$F_s = \frac{g_s A_r A_a}{A_a + \Sigma A_r}, \quad (3)$$

g_s being the statistical weight of the satellite's lower level, A_r the radiative transition rate from the satellite's doubly excited upper level, A_a the corresponding autoionization rate, ΣA_r the sum of all possible radiative transition rates from the upper level, and E_s the satellite's transition energy. Values of I_s for *j* were calculated using the atomic data of Lemen et al. (1984).

The inner shell $n = 2$ satellites (e.g., *q*) have intensities given by

$$I'_s = \frac{N(\mathrm{Fe}^{+23})N_e V}{4\pi(1\ \mathrm{AU})^2}\frac{8.63\times10^{-6}\Upsilon_s\exp(-E_s/k_\mathrm{B}T_e)}{T_e^{1/2}}\ \mathrm{photons\ cm^{-2}\ s^{-1}}, \quad (4)$$

where $N(\mathrm{Fe}^{+23})$ is the number density of Fe^{+23} ions $(=[N(\mathrm{Fe}^{+23})/N(\mathrm{Fe})]A_{\mathrm{flare}}(\mathrm{Fe})N(\mathrm{H}))$ and Υ_s is the temperature-averaged collision strength of the satellite line transition. There is hence a T_e dependence through the ionization fraction $N(\mathrm{Fe}^{+23})/N(\mathrm{Fe}^{+24})$. Values of I'_s were calculated using data of Lemen et al. (1984) and ionization fractions of Mazzotta et al. (1998).

Similar expressions to these give the intensities of satellites, dielectronic or inner shell, emitted by lower Fe ionization stages (Fe XIX–Fe XXIII: 6.50–6.62 keV) but with ionization fractions $N(\mathrm{Fe}^{+18})$ to $N(\mathrm{Fe}^{+22})$. The Fe XIX–Fe XXII are generally much weaker than the Fe XXIV satellites. The intensities of the Fe XXIII lines are more significant; line β, due mostly to inner shell excitation, was calculated as representative of other Fe XXIII satellites.

The Fe fluorescence Kα lines (6.387, 6.400 keV) formed in or near the photosphere have intensity $I_{\mathrm{K}\alpha}$ given by (Bai 1979)

$$I_{\mathrm{K}\alpha} = \frac{\Gamma(h) f(h,\theta)}{1+\alpha(h,\theta)} \int_{I_{\mathrm{K}}}^{\infty} I_c^{\mathrm{tot}}(E)\, dE. \quad (5)$$

Here Γ is the Kα fluorescence efficiency (ratio of emitted Kα photons s^{-1} to $\frac{1}{2}\int_{I_{\mathrm{K}}}^{\infty} I_c^{\mathrm{tot}}\, dE$, where I_c^{tot} is the total continuum flux at Earth); $f(h,\theta)$ is a factor expressing the dependence of $I_{\mathrm{K}\alpha}$ on θ, the heliocentric angle between the observer and flare, and its height h above the photosphere; and α is an albedo factor allowing for the amount of continuum radiation Compton scattered by the photosphere. We can take I_c^{tot} to be the thermal bremsstrahlung spectrum,

$$I_c(E,T_e) = 1.03\times10^{-11}\, \frac{g_c \exp(-E/k_{\mathrm{B}}T_e)}{E T_e^{1/2}}\, \frac{N_e N(\mathrm{H}) V}{4\pi(1\ \mathrm{AU})^2}, \quad (6)$$

where g_c is the free-free Gaunt factor, of order 1 (Mewe, Gronenschild, & van den Oord 1985a). Both Γ and α are slowly decreasing functions of h. For typical flare heights $h = 10,000$–$30,000$ km and a photospheric Fe abundance [$A_{\mathrm{ph}}(\mathrm{Fe}) = N(\mathrm{Fe})/N(\mathrm{H}) = 3.2\times10^{-5}$; Grevesse & Sauval 1998], $\Gamma \approx 0.015\% \pm 20\%$, $\alpha \approx 0.06 \pm 0.02$, $f(h,\theta=0) = 1.5 \pm 0.05$, and so for a typical flare at Sun center, the Fe Kα line intensity is

$$I_{\mathrm{K}\alpha} = 5.4\times10^{-5}\, \frac{N_e N(\mathrm{H}) V}{4\pi(1\ \mathrm{AU})^2}\, \frac{A_{\mathrm{ph}}(\mathrm{Fe}) g_c E_1(I_{\mathrm{K}}/k_{\mathrm{B}}T_e)}{T_e^{1/2}}, \quad (7)$$

where E_1 is the first logarithmic integral. This equation was used to calculate $I_{\mathrm{K}\alpha}$ with T_e assumed to be the temperature of the flare plasma, i.e., that used in equations (1), (2), and (4). The Fe Kβ lines (7.05–7.10 keV) have an intensity of $\sim 0.13 I_{\mathrm{K}\alpha}$.

Finally, the Fe XXVI Lyα doublet (6.947, 6.969 keV) contributes significantly to the Fe line feature at $T_e \gtrsim 30$ MK. Like Fe XXV line *w*, the lines are mainly collisionally excited, with small contributions made by cascades. Data extrapolated from Aggarwal & Kingston (1993) were used to calculate the intensities. High-*n* satellites, spectroscopically indistinguishable from the Lyα lines, contribute to the total intensity, up to 30% at $T_e = 20$ MK. The intensities of Fe XXV satellites like those making up *J* (6.920 keV) were calculated with expressions similar to equation (2), using data from Dubau et al. (1981).

Figure 1 shows the contributions, as a function of T_e, of the individual lines mentioned above to the Fe line feature. The "total" emission in the Fe line feature in this figure is given by the sum of all lines in the 5.8–7.5 keV range except the Fe Kα and Kβ lines from the Chianti atomic database and code (ver. 4.2). Figure 1 shows that for $T_e \lesssim 70$ MK Fe XXV line *w* dominates, and for $T_e \gtrsim 85$ MK the Fe XXVI Lyα lines are the largest contributor. The maximum of the total curve is at $T_e \sim 75$ MK, far higher than the range (approximately 20–30 MK) of the thermal component of most solar flares. The summed intensity of Fe XXIV dielectronic satellites exceeds the intensity of line *w* for $T_e \lesssim 15$ MK. For T_e as high as 30 MK, the contribution of dielectronic satellites like *j* is a significant fraction of I_w. Satellite *q*, the most intense of the inner shell satellites, is comparable to *j*. Satellite emission from lower stages adds only a small amount of emission at $T_e \lesssim 20$ MK. Satellite feature *J* near the Fe XXVI Lyα lines is comparable to the intensity of the Fe XXVI lines for $T_e \lesssim 30$ MK, but at these temperatures, Fe XXV line *w* dominates.

For the coronal (Feldman & Laming 2000) abundances assumed here, the photospheric Fe Kα lines make only a small ($\lesssim$4%) contribution to the total in this temperature range, but the contribution increases with T_e because of the increase of $\int_{I_{\mathrm{K}}}^{\infty} I_c^{\mathrm{tot}}(E)\, dE$. Moreover, for a flare plasma with photospheric Fe abundance (as with the impulsive *Skylab* flare cited by Feldman & Laming 2000), i.e., one with $A_{\mathrm{flare}}(\mathrm{Fe})$ that is $\sim$0.25 times less than the coronal value assumed above, all the contribution functions in Figure 1 are decreased by a factor of 4 compared with the Fe Kα curve; the Fe Kα lines will then be as much as $\sim$15% of the total at $T_e = 100$ MK.

The most intense lines making up the Fe/Ni line feature (7.5–9.2 keV) are the Fe XXV $1s^2$–$1snp$ and Fe XXVI $1s$–np ($n \geq 3$) lines, which are, like the $n = 2$ lines, collisionally excited and so have intensities given by equation (1) with Υ appropriate for each transition. We took the Fe XXV $1s^2$–$1s3p$ and Fe XXVI $1s$–$3p$ lines as representative of all transitions, using data of Pradhan (1985) and Aggarwal & Kingston (1993). Satellites to the Fe XXV $1s^2 = 1s3p$ line are also important contributors at relatively low temperatures. We calculated the sum of all significant satellites to the $1s^2$–$1s3p$ line using the atomic data of M. Cornille (Kato et al. 1997). The Fe/Ni line feature also includes Ni XXVII $1s^2$–nl ($n = 2$, 3; $l = s$, p: 7.73–9.177 keV); the data of Zhang & Sampson (1987) and Harra-Murnion et al. (1995) were used to calculate their intensities. For the Ni XXVIII Lyα doublet (8.096, 8.067 keV), we used the Aggarwal & Kingston (1993) Fe XXVI data extrapolated to H-like Ni. Lines of Ni are less intense than the equivalent Fe lines because the Ni abundance (coronal or photospheric) is a factor of 20 smaller than that of Fe. Hence, we omit the fluorescence-formed Ni lines. We note that the energy range of the Fe/Ni line feature includes the Fe XXV recombination edge at 8.829 keV, which contributes to the total emission when the continuum is included.

Figure 2 shows the contributions of individual lines to the Fe/Ni line feature as a function of T_e. "Total" emission is the sum of all lines in the range 7.5–9.2 keV from Chianti. This figure shows that the major part of the Fe/Ni line feature is made up of the Fe XXV $1s^2$–$1s3p$ ($T_e \lesssim 80$ MK) and the Fe XXVI Lyβ lines. At temperatures $T_e \lesssim 18$ MK, satellites to the Fe XXV

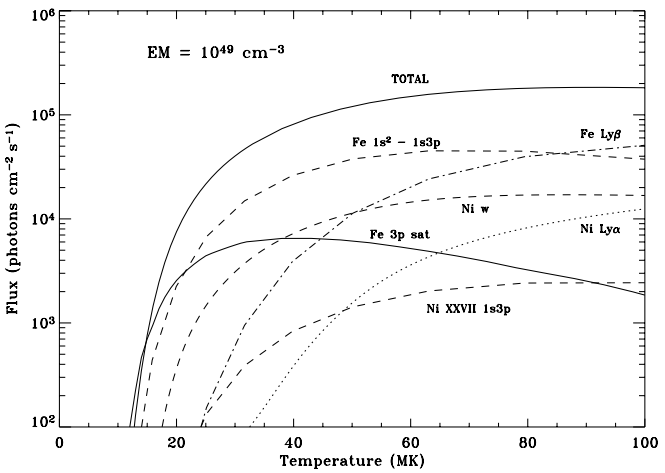

FIG. 2.—Contribution of principal emission lines (labeled) making up the 8 keV Fe/Ni line feature. The curve labeled "Total" is the total emission in the line feature between 7.5 and 9.2 keV as estimated from Chianti (ver. 4.2). Curves marked "Ni w" and "Ni Lyα" are those for the Ni XXVII *w* line and the Ni XXVIII Lyα doublet. The curve marked "Fe 3p sat" is for the sum of satellites to the Fe XXV $1s^2$–$1s3p$ line. Fluxes are given for an emission measure of 10^{49} cm^{-3}.

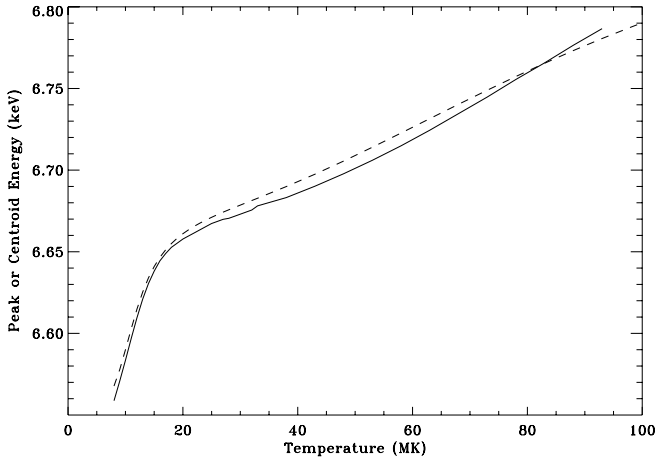

FIG. 3.—Peak (*solid line*) and centroid (*dashed line*) energies as a function of T_e of the Fe line feature observed by a spectrometer like *RHESSI*, having FWHM = 0.8 keV resolution.

$1s^2$–$1s3p$ lines are dominant. They are not included in version 4.2 of Chianti; hence, the "Total" curve departs from the sum of the largest contributors to the Fe/Ni line feature at these temperatures. The Ni XXVII line *w* is only 15% of the intensity of the Fe XXV line at $T_e \sim 20$ MK. The contribution of all Ni XXVII, Ni XXVIII lines and their satellites is never more than about 25% of the total, so the Fe/Ni line feature is in fact mostly made up of Fe lines.

2.3. *Centroid and Peak Energies of the* Fe *Line Feature*

The Fe line and Fe/Ni line features as viewed by a broadband spectrometer like *RHESSI* are thus made up of many individual lines each having its own temperature dependence. Their contribution to the total emission of either the Fe line or Fe/Ni line feature will therefore change as the temperature of a solar flare plasma changes in both space and time. This results in changes to the energies of the Fe line and Fe/Ni line features, as defined by the energy of the peak intensity (E_p) or centroid energy [$E_c = \int EI(E)\,dE / \int I(E)\,dE$, where $I(E)$ is spectral intensity at energy E, integrals over the range of each line feature]. Changes in E_p and E_c, if large enough, therefore provide a possible useful temperature diagnostic. We assume that the continuum contribution to the spectrum has been subtracted. As the Fe/Ni line feature is relatively weak, we examine only the case of the Fe line feature.

For the Fe XXV lines and their satellites, increasing T_e results in decreasing the intensities of satellites, both dielectronic and inner shell, relative to line *w*. For lower temperatures, when Fe XXVI line emission is insignificant, E_p and E_c should be less than the energy of line *w* (6.699 keV), but increasing slightly with T_e as the dielectronic and inner shell satellites decrease relative to line *w*. For higher temperatures, for which there is significant Fe XXVI line (6.952, 6.973 keV) emission, E_p or E_c is expected to shift to energies greater than line *w*. Unless the flare abundance of Fe is much less than the coronal value, the Fe Kα lines (6.404, 6.391 keV) are always too weak to produce a countereffective shift of E_p or E_c to lower energies through their increase during the flare rise.

Synthetic spectra from the Chianti code in the 3.8–10 keV range were used to find changes in E_p and E_c with T_e. The spectra, which are given in terms of wavelength, were first synthesized without continuum contributions at 1 MK intervals and transformed to an energy scale. They were then convolved with a Gaussian curve having an FWHM of 0.8 keV to match the spectral resolution of detector 4 of *RHESSI*. The derived values of E_p and E_c (different by $\lesssim$0.01 keV) are plotted against T_e in Figure 3. The Fe line feature is very weak when $T_e \lesssim 12$ MK. At higher T_e, there is a slow rise in E_p and E_c from 6.63 to 6.70 keV over the range $T_e = 15$–45 MK as the Fe XXIV satellites decrease relative to line *w*. For $T_e \gtrsim 45$ MK, the rise with T_e is slightly accelerated as the Fe XXVI Lyα lines become more significant. The rise of E_p and E_c over the temperature range of most flares, although modest, is barely measurable with *RHESSI*; although the energy resolution at 7 keV is 0.8 keV, Gaussian fitting techniques enable the peak and centroid energies to be defined to $\sim$0.01 keV for strong events. However, an unexpected change of gain with count rate in the *RHESSI* detectors has made this goal unachievable at present.

A check on the validity of Figure 3 for $T_e \lesssim 35$ MK is provided by high-resolution flare observations of the Fe line feature made with the *SMM* Bent Crystal Spectrometer (energy range 6.4–7.0 keV) and the *Yohkoh* Bragg Crystal Spectrometer (6.6–7.1 keV). Two very large flares (1980 July 1, seen by *SMM*, and 1991 December 16, seen by *Yohkoh*) were selected for which Fe XXVI line emission was detected. The *SMM* spectrometer energy range includes satellite lines from lower Fe ionization stages. Its high resolving power ($\Delta E/E \sim 4000$) enabled accurate I_j/I_w line ratios to be obtained, leading to temperature uncertainties $\Delta T_e \sim \pm 0.5$ MK. The spectra from the *Yohkoh* instrument, although having lower resolution ($E/\Delta E \sim 1000$), can nevertheless be analyzed with spectral fitting routines to give $\Delta T_e = \pm 0.5$ MK uncertainties. Several spectra over the course of each flare were convolved with a Gaussian filter having FWHM = 0.8 keV, first subtracting an instrumental background that is present and dominates over the continuum. From this, E_c and E_p were derived. The values of these energies have uncertainties of about 0.02 keV. Figure 4 is a plot of observed values of E_c and T_e compared with the dashed curve of Figure 3 derived from Chianti spectra. Most of the observed points agree with the curve to within the uncertainties defined by the error bars, adequate to show the predicted increase of E_c with T_e over this temperature range. This comparison confirms the validity of the Chianti

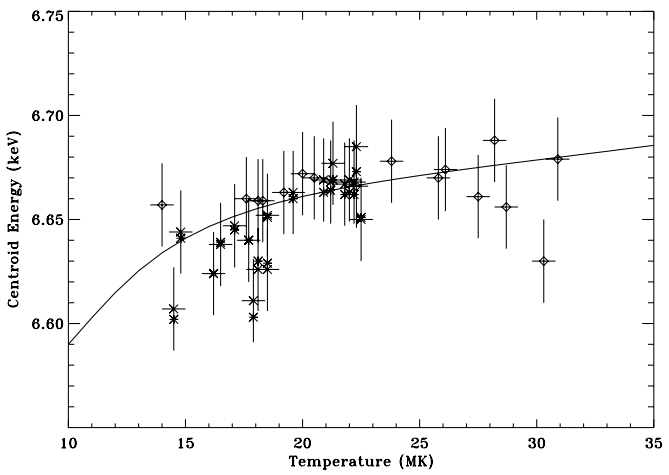

FIG. 4.—Centroid energy of the Fe line feature, observed with a spectrometer like *RHESSI* having a resolution with FWHM 0.8 keV, compared with observed points from the *SMM* Bent Crystal Spectrometer (*asterisks*) and the *Yohkoh* Bragg Crystal Spectrometer (*diamonds*) for large flares on 1980 July 1 and 1991 December 16, respectively.

synthetic spectra in this range, as well as the diagnostic potential of E_p or E_c of flare temperature.

2.4. *Intensity Ratio of* Fe *Line and* Fe/Ni *Line Features*

The differing T_e sensitivity of the Fe line and Fe/Ni line features (Figs. 1 and 2) means that the ratio of the features offers another method for determining T_e in addition to the peak or centroid energies of the Fe line feature. The intensity ratio, derived from Chianti but adding the intensity of satellites to the Fe XXV $1s^2$–$1s3p$ line that are omitted from Chianti, is shown in Figure 5. The intensity ratio decreases by almost a factor of 2 from 20–30 MK, but at higher temperatures it decreases much more slowly. This intensity ratio as a temperature diagnostic may therefore be of only limited use.

3. LINE AND CONTINUUM EMISSION

3.1. *Synthetic* 3.8–10 keV *Spectra*

As indicated in § 1, the Fe line and Fe/Ni line features are observed as emission excesses above a thermal continuum that decreases with photon energy E. Most of this continuum is bremsstrahlung emission, and approximately 90% of this is from hydrogen. For $T_e \lesssim 20$ MK, free-bound emission contributes significantly to the 3.8–10 keV energy range but is progressively less important for higher T_e (Culhane 1969; Mewe et al. 1985a). Much of the free-bound emission is from higher Z elements like Fe and Ca. Two-photon continuum emission (from the radiative decay of metastable atomic states) is always negligible. The thermal continuum from the Chianti code is within 1% of the detailed calculations of Culhane (1969) and the approximations of Mewe et al. (1985a), so we use the Chianti calculations throughout this section.

Figure 6 shows the synthetic spectra from Chianti in the 4.6–9.1 keV range for 8 MK $< T_e <$ 33 MK in 1 MK intervals. The original line and continuum spectrum for each temperature has been transformed to an energy (keV) scale and a flux scale with fluxes in photon cm^{-2} s^{-1} keV^{-1}. Coronal element abundances (Feldman & Laming 2000) and the ion fractions of Mazzotta et al. (1998) were used. The spectra were convolved with a 0.8 keV FWHM Gaussian, matching the spectral resolution of *RHESSI* detector 4. These synthetic spectra show the progressive intensity increase of the Fe line and Fe/Ni line features above the continuum with increasing T_e. The Fe line feature becomes visible above the continuum

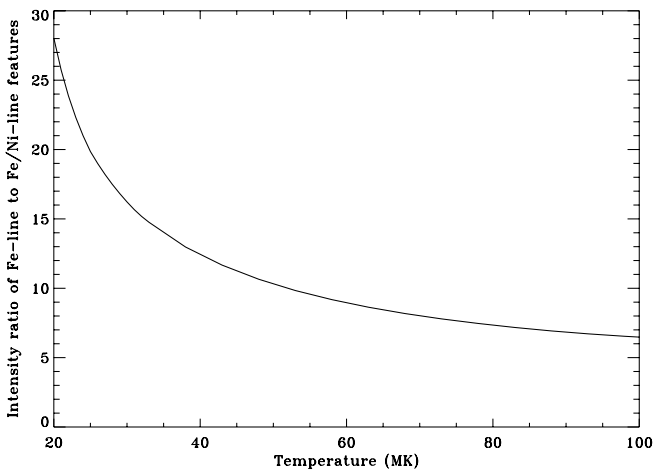

FIG. 5.—Intensity ratio of the Fe line and Fe/Ni line features as a function of T_e.

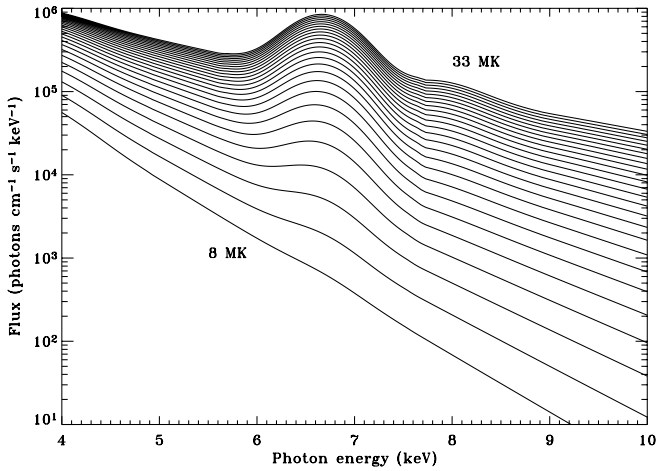

FIG. 6.—Synthetic spectra between 4 and 10 keV from the Chianti code, with coronal abundances of Fe and Ni, smoothed with a Gaussian filter having FWHM = 0.8 keV. Spectra are given in 1 MK intervals from 8 to 33 MK. Fluxes are those at the mean solar distance and for a flare with volume emission measure $\int_V N_e^2\, dV = 10^{49}$ cm^{-3}.

only when $T_e \gtrsim 10$ MK. This is in agreement with Figure 1 and *SMM* and *Yohkoh* Bragg Crystal Spectrometer observations (Fig. 4). Empirically determined Fe^{+24}–Fe^{+25} ionization fractions from *SMM* observations (Antonucci et al. 1987) are in better agreement with calculations by Mazzotta et al. (1998) and Arnaud & Raymond (1992), based on improved ionization and recombination data, than the earlier Arnaud & Rothenflug (1985) work used extensively until the early 1990s, which indicated a significant Fe^{+24} fraction at $T_e \sim 10$ MK. Note that routines calculating X-ray emission and temperatures in the SolarSoft package (e.g., using SPEX or from *GOES* channel ratios) are still based on the Arnaud & Rothenflug (1985) ionization fractions, so caution should be used in results derived from them at low temperatures.

3.2. *Centroid and Peak Energies of* Fe *Line Feature with Continuum*

The centroid and peak energies of the Fe line and Fe/Ni line features in § 2.3 are given on the assumption that the continuum can be accurately subtracted in observed spectra. For some instruments this may not be the case. We therefore repeat the analysis with the continuum included, again using the Chianti code. Figure 7 shows these energies plotted against T_e. The variations of E_p and E_c are markedly different from those shown in Figure 3 at lower temperatures as the continuum is then so steeply declining with T_e that the centroid and peak energies, when defined with a Gaussian filter of 0.8 keV FWHM, are significantly influenced by the continuum, which is much more intense on the lower energy side of the Fe line feature than on the higher energy side. This explains the steep falloff of centroid and more particularly of the peak energy of the Fe line feature toward lower T_e. As can be seen from Figure 6, a maximum in the energy range 5.8–7.5 keV can only be defined for $T_e > 11$ MK.

3.3. *Abundance of* Fe *in Flare Plasmas: Equivalent Width*

The observation of the Fe line feature and neighboring continuum offers a means of determining the iron abundance $A_{\rm flare}$(Fe) during flares. The thermal plasma during flares is located in the coronal loop structures typically 10^4 km above the photosphere. On a chromospheric evaporation picture, this

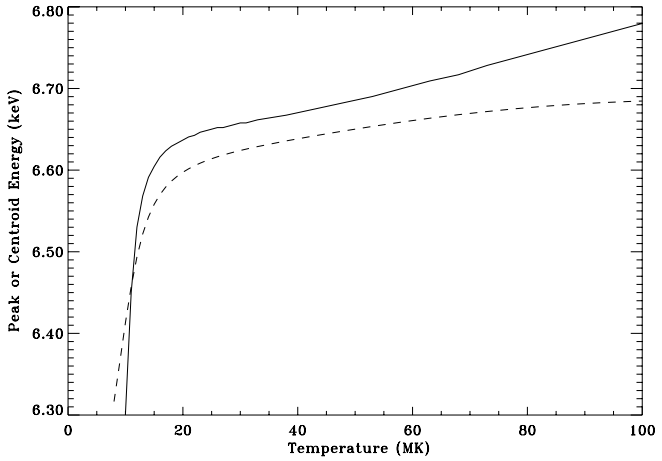

FIG. 7.—Peak (*solid line*) and centroid (*dashed line*) energies of the Fe line feature with continuum included plotted as a function of T_e. The energies have been derived assuming a Gaussian filter with FWHM = 0.8 keV.

plasma is formed from the chromosphere and so should reflect the chromospheric composition. Most analyses of flare X-ray and ultraviolet spectra (e.g., Fludra & Schmelz 1999; Phillips et al. 2003) show that elements with a variety of first ionization potentials (FIPs) are in ratios that are characteristic of the corona, i.e., with low-FIP (FIP $\lesssim$ 10 eV) elements enhanced by a factor of 3 or 4 but with high-FIP elements approximately the same or depleted by up to a factor of 2 compared with photospheric abundances. However, Feldman & Laming (2000) cite the case of a short-lived flare event observed with the *Skylab* ultraviolet spectrometer, which showed photospheric abundances. In addition, observations from *SMM* (Sylwester, Lemen, & Mewe 1984) indicate significant flare-to-flare variations. It is possible, then, that flare abundances are related to flare duration or some property that is determined by the nature of the chromospheric evaporation or other process that gives rise to the thermal plasma contained in coronal loops in flares. Since both Fe and Ni are low-FIP elements, *RHESSI* observations of the Fe line feature with neighboring continuum that allow the flare Fe abundance to be determined will give a valuable new diagnostic tool.

A measure of the Fe line feature's intensity with respect to the continuum is provided by the equivalent width, measured in keV, which can be determined from *RHESSI* spectra. Chianti spectra convolved with a Gaussian of FWHM 0.8 keV to simulate the spectral resolution of detector 4 of *RHESSI* permit the theoretical equivalent width to be determined as a function of T_e. Figure 8 shows this for $A_{\rm flare}$(Fe) equal to the coronal value. *RHESSI* observations of the flare thermal component can be analyzed to give T_e with fitting programs comparing the model and measured continuum spectra. Comparison of the equivalent width at an observed T_e with that calculated from Figure 8 should give $A_{\rm flare}$(Fe) in terms of the coronal abundance. Alternatively, if a value of $A_{\rm flare}$(Fe) can be assumed, then the equivalent width gives an estimate of the plasma temperatures. A plot of the equivalent width of what is essentially the Fe line feature, given by Rothenflug & Arnaud (1985), peaks at a lower T_e with a maximum value lower than that in Figure 8. The differences appear to be due to the different iron abundance (equal to the photospheric value, a factor of 4 less than coronal as used here) and ionization fractions (those of Arnaud & Rothenflug 1985). However, *Ginga* X-ray observations of flares on the Algol eclipsing binary star system indicate much smaller equivalent widths of the Fe line feature, implying much smaller Fe abundances relative to the solar coronal or even photospheric abundances.

4. IONIZATION CONDITIONS IN FLARES

Equations (1), (2), and (4) assume a steady state ionization equilibrium in the flare plasma. However, since temperature changes, particularly in the flare rise phase, are sometimes very rapid, the validity of this assumption might be questioned. If nonequilibrium conditions exist in flares, the plasma would be expected to be in an ionizing state during the rise phase, i.e., there are greater proportions of lower ionization stages than the instantaneous value of T_e would indicate. During the decay, the plasma is cooling and so would be expected to be in a recombining state, i.e., there are greater proportions of higher ionization stages. The time-dependent fraction of a particular ionization stage i ($N_i/N_{\rm Fe}$ in the case of Fe ions) is then governed by rate coefficients of ionization (Q) and recombination (α) rate coefficients from and to this stage:

$$\frac{1}{N_e}\frac{dN_i}{dT_e}\frac{dT_e}{dt} = Q_{i-1}N_{i-1} - N_i(Q_i + \alpha_i) + \alpha_{i+1}N_{i+1}, \quad (8)$$

with the observed temperature changes defined by dT_e/dt. Time-dependent calculations solving for N_i have been done for flare plasmas by Phillips, Neupert, & Thomas (1974) and Mewe et al. (1985b). They show that unless T_e changes are very rapid, i.e., $dT_e/dt \gtrsim 5\times10^5$ K s^{-1}, ionization equilibrium is likely to be a good approximation unless $N_e \lesssim 10^{10}$ cm^{-3}. Mewe et al. (1985b) using chromospheric evaporation models show that time-dependent effects are significant for the impulsive stage, although the exact details depend on the dynamic effects included in the model.

This is illustrated for the case of the 1991 December 16 flare observed by *Yohkoh*, which was large but relatively short lived and therefore likely to show possible time-dependent effects. Figure 9 shows three curves, the Bragg crystal spectrometer light curve in the Fe XXV channel, T_e, and values of $(dT_e/dt)/T_e$ derived as a function of time from satellite-to-line w intensity ratios. Values of $(dT_e/dt)/T_e$ when T_e is rising

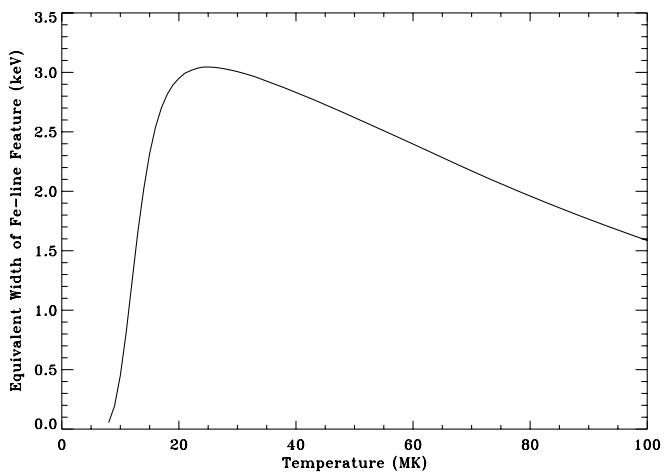

FIG. 8.—Equivalent width of the Fe line feature (keV) as a function of T_e, calculated from the Chianti code with the coronal abundances of Feldman & Laming (2000).

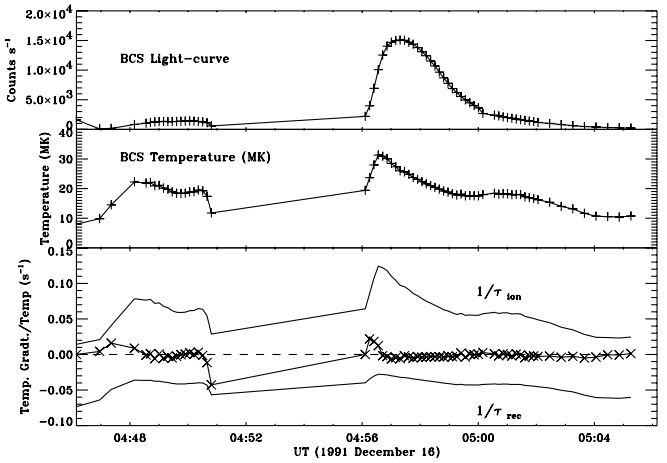

FIG. 9.—Light curve (*top panel*) and T_e (*middle panel*) from *Yohkoh* Bragg Crystal Spectrometer Fe XXV spectra, together with values of $(dT_e/dt)/T_e$ (*bottom panel*) derived from the temperature variations, for the large flare on 1991 December 16. Positive values of $(dT_e/dt)/T_e$, i.e., during temperature rise phases, are compared with inverse ionization times $1/\tau_{\rm ion}$ for $N_e = 10^{10}$ cm^{-3}, and negative values are compared with inverse recombination times $1/\tau_{\rm rec}$.

$(dT_e/dt > 0)$ are compared with inverse ionization times τ_i^{-1}, where

$$\tau_i = \frac{1}{Q_i N_e}, \tag{9}$$

Q_i being the rate coefficient (cm^3 s^{-1}) for ionization of Fe^{+23} to Fe^{+24} ions and N_e assumed to be 10^{10} cm^{-3}. Similarly, when T_e is falling, values of $(dT_e/dt)/T_e$ (<0) are compared with inverse recombination times τ_r^{-1}, where

$$\tau_r = \frac{1}{\alpha_i N_e}, \tag{10}$$

α_i being the rate coefficient for recombination of Fe^{+25} to Fe^{+24} ions and again $N_e = 10^{10}$ cm^{-3}. Figure 9 shows that the absolute values of $(dT_e/dt)/T_e$ are always less than either τ_i^{-1} or τ_r^{-1}; that is, the timescales for flare temperature changes are always more than the Fe^{+24} ionization and recombination times for $N_e = 10^{10}$ cm^{-3}. This holds a fortiori for larger densities (as are indicated by X-ray line ratios [e.g., Doschek et al. 1981; Phillips et al. 1996], immediately after the impulsive stage), which give correspondingly shorter ionization and recombination times.

An isothermal plasma is implicit in equations (1), (2), and (4) and in the discussion so far, but more realistically the plasma has a nonthermal temperature structure, describable by a differential emission measure (DEM), $\phi(T_e) = N_e^2\, dV/dT_e$. Procedures for deriving the flare DEM from crystal spectrometer data are outlined by Fludra & Schmelz (1999), but for flare spectra observed by *RHESSI* one must resort to DEMs from flare loop models (McTiernan, Fisher, & Li 1999) or analytical approximations with parameters from the continuum slope (Phillips et al. 2003). Imaging spectroscopy also provides another tool to separate plasma with different temperatures and allow the DEM to be determined spectroscopically.

5. SUMMARY AND APPLICATIONS TO NONSOLAR SOURCES

The 3.8–10 keV spectral region of solar flares includes atomic lines from highly stripped ions of elements such as Ca, Fe, and Ni, having the largest excitation energies of any atomic transitions of cosmically abundant elements. These lines potentially provide diagnostic information about the hottest plasma produced during flares. Table 1 gives details of the principal lines over the 3.8–10 keV range. Two line groups, centered on ~7 and ~8 keV, are made up largely of Fe lines but with some Ni line emission at ~8 keV. With a broadband instrument (energy resolution ~0.8 keV) such as *RHESSI* or *NEAR* PIN, these groups of lines form line features called here the Fe line and Fe/Ni line features, defined by excess emission over the continuum in the ranges 5.8–7.5 and 7.5–9.2 keV, respectively. An instrument like *RHESSI* could use the peak or centroid energies (E_p or E_c) of the more intense Fe line feature to determine T_e for comparison with that found from the continuum slope, assumed thermal in origin. In addition, the thermal and nonthermal components of the measured continuum spectrum can be more cleanly separated if temperature and emission measure can be independently determined from the two line complexes. The fluorescence-formed Fe Kα lines make only a very small contribution to the Fe line feature at these temperatures, but this contribution increases with T_e. In principle, the intensity ratio of the Fe line and Fe/Ni line features is temperature sensitive, but this ratio is only useful if the Fe/Ni line feature is easily measurable. The equivalent width of the Fe line feature gives the best temperature diagnostic. However, the equivalent width also depends on the Fe abundance in the flaring plasma; this may vary from flare to flare, possibly also during the course of each flare. The calculated equivalent widths given here assume coronal abundances, where the abundances of low-FIP elements like Fe and Ni are taken to be 4 times photospheric. If T_e can be determined from the flare continuum slope (nonthermal contribution in the 3.8–10 keV range assumed to be negligible), the equivalent width of the Fe line can then be used to investigate possible Fe abundance variations. Finally, we show that in spite of rapidly varying T_e during flares, ionization equilibrium can be assumed for Fe ions in most circumstances.

The results here should be applicable to nonsolar X-ray–emitting plasmas such as those formed in stellar flares, the hot gas in some galaxies and clusters of galaxies, and older supernova remnants, or for any source for which photoionization contributes little to the ionization equilibrium. They would not be applicable to X-ray sources such as X-ray binaries, some active galactic nuclei, and recent supernova remnants where there is a strong photoionizing continuum present. Spectrometers aboard the *EXOSAT*, *Ginga*, and *Tenma* spacecraft had spectral resolutions of about 1 keV at ~7 keV, so the results given here could be applied to their spectra. Higher resolution spectrometers now operating on the *Chandra* and *XMM-Newton* spacecraft (FWHM of energy resolution ~200 eV at the Fe line feature's energy) are partially able to resolve the satellite structure of the Fe lines and so will obtain better temperature and abundance information than for broadband instruments.

This research was made possible through a National Research Council Research Associateship award at NASA Goddard Space Flight Center. Cristina Chifor, Brian R. Dennis, Enrico Landi, Hugh Hudson, and Janusz Sylwester are sincerely thanked for their contributions to this paper. Chianti is a collaborative project involving Naval Research Laboratory, Rutherford Appleton Laboratory (UK), and the Universities of Florence (Italy) and Cambridge (UK).

REFERENCES

Acton, L. W., et al. 1980, Sol. Phys., 65, 53
Aggarwal, K. M., & Kingston, A. E. 1993, ApJS, 85, 187
Antonucci, E., Dodero, M. A., Gabriel, A. H., Tanaka, K., & Dubau, J. 1987, A&A, 180, 263
Arnaud, M., & Raymond, J. 1992, ApJ, 398, 394
Arnaud, M., & Rothenflug, R. 1985, A&AS, 60, 425
Bai, T. 1979, Sol. Phys., 62, 113
Bely-Dubau, F., Dubau, J., Faucher, P., & Gabriel, A. H. 1982, MNRAS, 198, 239
Bitter, M., et al. 1979, Phys. Rev. Lett., 43, 129
———. 1991, Phys. Rev. A, 44, 1796
Boiko, V. A., Pikuz, S. A., Safronova, U. I., & Faenov, A. Ya. 1978, MNRAS, 185, 789
Bombarda, F., et al. 1988, Phys. Rev. A, 37, 504
Culhane, J. L. 1969, MNRAS, 144, 375
Culhane, J. L., et al. 1991, Sol. Phys., 136, 89
Dere, K. P., Landi, E., Mason, H. E., Monsignori Fossi, B. C., & Young, P. R. 1997, A&AS, 125, 149
Doschek, G. A., Feldman, U., Kreplin, R. W., & Cohen, L. 1980, ApJ, 239, 725
Doschek, G. A., Feldman, U., Landecker, P. B., & McKenzie, D. L. 1981, ApJ, 245, 315
Doschek, G. A., Kreplin, R. W., & Feldman, U. 1979, ApJ, 233, L157
Doschek, G. A., & Meekins, J. F. 1973, in High Energy Phenomena on the Sun, ed. R. Ramaty & R. G. Stone (NASA SP-342; Greenbelt: GSFC), 262
Doschek, G. A., Meekins, J. F., Kreplin, R. W., Chubb, T. A., & Friedman, H. 1971, ApJ, 170, 573
Dubau, J., Gabriel, A. H., Loulergue, M., Steenman-Clark, L., & Volonté, S. 1981, MNRAS, 195, 705
Emslie, A. G., Phillips, K. J. H., & Dennis, B. R. 1986, Sol. Phys., 103, 89
Erickson, G. W. 1977, J. Phys. Chem. Ref. Data, 6, 831
Ermolaev, A. M., & Jones, M. 1973, J. Phys. B, 6, 1
Feldman, U., Doschek, G. A., Mariska, J. T., & Brown, C. M. 1995, ApJ, 450, 441
Feldman, U., & Laming, M. 2000, Phys. Scr., 61, 222
Fludra, A., & Schmelz, J. T. 1999, A&A, 348, 286
Gabriel, A. H. 1972, MNRAS, 160, 99
Grevesse, N., & Sauval, A. J. 1998, Space Sci. Rev., 85, 161
Harra-Murnion, L. K., Boone, A. W., Keenan, F. P., Kingston, A. E., & Norrington, P. H. 1995, Phys. Scr., 51, 346
Hata, J., & Grant, I. P. 1982, MNRAS, 198, 1081
———. 1984, MNRAS, 211, 549
Kato, T., Safronova, U. I., Shlyaptseva, A. S., Cornille, M., Dubau, J., & Nilsen, J. 1997, At. Data Nucl. Data Tables, 67, 225
Kimura, E. Nakazaki, S., Berrington, K. A., & Norrington, P. H. 2000, J. Phys. B, 33, 3449
Lemen, J. R., Phillips, K. J. H., Cowan, R. D., Hata, J., & Grant, I. P. 1984, A&A, 135, 313
Lin, R. P., et al. 2002, Sol. Phys., 210, 3
Masuda, S., Kosugi, T., Hara, H., Tsuneta, S., & Ogawara, Y. 1994, Nature, 371, 495
Mazzotta, P., Mazzitelli, G., Colafrancesco, S., & Vittorio, N. 1998, A&AS, 133, 403
McTiernan, J. M., Fisher, G. H., & Li, P. 1999, ApJ, 514, 472
Mewe, R., Gronenschild, E. H. B. M., & van den Oord, G. H. J. 1985a, A&AS, 62, 197
Mewe, R., Lemen, J. R., Peres, G., Schrijver, J., & Serio, S. 1985b, A&A, 152, 229
Neupert, W. M. 1971, Sol. Phys., 18, 474
Neupert, W. M., & Swartz, M. 1970, ApJ, 160, L189
Palmeri, P., Mendoza, C., Kallman, T. R., Bautista, M. A., & Meléndez, M. 2003, A&A, 410, 359
Parmar, A. N., Culhane, J. L., Rapley, C. G., Wolfson, C. J., Acton, L. W., Phillips, K. J. H., & Dennis, B. R. 1984, ApJ, 279, 866
Phillips, K. J. H., Bhatia, A. K., Mason, H. E., & Zarro, D. M. 1996, ApJ, 466, 549
Phillips, K. J. H., Lemen, J. R., Cowan, R. D., Doschek, G. A., & Leibacher, J. W. 1983, ApJ, 265, 1120
Phillips, K. J. H., & Neupert, W. M. 1973, Sol. Phys., 32, 209
Phillips, K. J. H., Neupert, W. M., & Thomas, R. J. 1974, Sol. Phys., 36, 383
Phillips, K. J. H., Pike, C. D., Lang, J., Watanabe, T., & Takahashi, M. 1994, ApJ, 435, 888
Phillips, K. J. H., Rainnie, J. A., Harra, L. K., Dubau, J., Keenan, F. P., & Peacock, N. 2004, A&A, in press
Phillips, K. J. H., Sylwester, J., Sylwester, B., & Landi, E. 2003, ApJ, 589, L113
Pradhan, A. 1985, ApJS, 59, 183
Rothenflug, R., & Arnaud, M. 1985, A&A, 144, 431
Sevier, K. D. 1979, At. Data Nucl. Data Tables, 24, 323
Spitzer, L. 1962, Physics of Fully Ionized Gases (New York: Wiley)
Starr, R., et al. 2000, Icarus, 147, 498
Sylwester, J., Culhane, J. L., Doschek, G. A., Oraevsky, V. N., Phillips, K. J. H., & Sylwester, B. 2002, in Solar Variability: From Core to Outer Frontiers, ed. A. Wilson (ESA SP-506; Noordwijk: ESA), 765
Sylwester, J., Lemen, J. R., & Mewe, R. 1984, Nature, 310, 665
Tanaka, K. 1986, PASJ, 38, 225
Yoshimori, M., et al. 1991, Sol. Phys., 136, 69
Young, P. R., Del Zanna, G., Landi, E., Dere, K. P., Mason, H. E., & Landini, M. 2003, ApJS, 144, 135
Zhang, H., & Sampson, D. H. 1987, ApJS, 63, 487